ELSEVIER

Journal of Power Sources 83 (1999) 121–127

JOURNAL OF POWER SOURCES

www.elsevier.com/locate/jpowsour

Cobalt doped chromium oxides as cathode materials for secondary lithium batteries

Dong Zhang [a], Branko N. Popov [a,*], Yury M. Podrazhansky [b], Pankaj Arora [a], Ralph E. White [a]

[a] *Center for Electrochemical Engineering Department of Chemical Engineering University of South Carolina, Columbia, SC 29208 USA*
[b] *Advanced Charger Technology, Technology Park — Atlanta Norcross, GA 30092 USA*

Received 15 January 1999; accepted 31 March 1999

Abstract

Cobalt doped chromium oxides were synthesized and characterized as cathode materials for secondary lithium batteries. A small amount of Co as dopant in the chromium oxides provides greater stability to the structure of CrO_x and helps in improving the high-rate behavior of these oxides. Optimized $Co_{0.2}CrO_x$ exhibited an initial capacity of 290 mA h/g with an average discharge voltage of 3.0 V vs. Li/Li^+. The lithiated $Co_{0.2}CrO_x$ exhibited an initial capacity of 230 mA h/g. Both lithiated and non-lithiated $Co_{0.2}CrO_x$ were found to be reversible in the entire intercalation range (2.0–4.2 V vs. Li/Li^+). Compared with pure CrO_x, Co doped CrO_x is characterized by better high-rate behavior (> 85% capacity for $Co_{0.2}CrO_x$ and > 75% capacity for $LiCo_{0.2}CrO_x$ at 0.65 C discharge rate). © 1999 Elsevier Science S.A. All rights reserved.

Keywords: Doped chromium oxides; Cobalt; Lithium; Cathode; Lithium-ion batteries

1. Introduction

The most prominent cathode material used in Lithium-ion industry is $LiCoO_2$, in spite of its high cost [1]. This is because of its stability and reversibility in the entire intercalation region and very small fade in capacity during cycling. The other two prominent cathode materials ($LiMn_2O_4$ and $LiNiO_2$) have not yet been commercialized because of various problems [2,3]. Recently, various substitutions (Co, Ni, Al, Cr etc.) on the transition metal site have been tried in $LiMn_2O_4$ and $LiNiO_2$ to improve the electrochemical and structural properties of these oxides [4–6]. The doped Co helps in stabilizing the structure of these oxides and reduces the capacity fade while compromising slightly on the overall capacity [4]. Vanadium oxides are also promising cathode materials because of their high initial capacity (300 mA h/g or higher) [7–9]. The shape of voltage plateau and cycling life needs to be improved before they can be used in commercial lithium batteries.

Chromium oxides (CrO_x) are promising cathode materials for secondary lithium batteries [10–12]. Recently, Arora et al. [11] showed that they exhibit high initial capacity (240–260 mA h/g) when cycled at 0.1 mA/cm^2 with an average discharge voltage of 3.0 V vs. Li/Li^+. Chemically modified chromium oxide was also used as a precursor to synthesize quaternary $LiCr_yMn_{2-y}O_4$ at high oxygen pressure [5]. The CrO_x doped spinel were more stable compared to Cr(III) doped spinel, both structurally and electrochemically.

The stoichiometry of the CrO_x samples was determined using a Perkin Elmer TGA7 thermal gravimetric analyzer. The O/Cr ratio was determined by reducing the CrO_x samples to Cr_2O_3 in air at 1°C/min. The decomposition of CrO_x to Cr_2O_3 starts at 385°C. The knowledge of final product stoichiometry (Cr_2O_3) and weight loss (corresponding to O_2 lost or evolved) lead to O/Cr ratio. The O/Cr ratio in CrO_x and $LiCo_{0.2}CrO_x$ were estimated to be 2.7 and 3.03, respectively. The purity of chromium oxides was found to depend on the synthesis pressure and temperature.

Both lithiated and non-lithiated chromium oxides (CrO_x) exhibit fade in capacity during cycling and poor high-rate behavior. The poor high-rate behavior can be attributed to a very small lithium diffusion coefficient in these oxides [13–15]. In the previous work we have optimized the synthesis conditions to produce a high capacity cathode

* Corresponding author. Tel.: +1-803-777-7314; fax: +1-803-777-8265; E-mail: popov@engr.sc.edu

PII: S0378-7753(99)00284-0

material (CrO_x) and characterized it both structurally and electrochemically. The capacity fades in CrO_x and $LiCrO_x$ indicated the structural instability of the material. This can be overcome, by doping CrO_x structure with foreign atoms like Co. In this work, we extend our research into the electrochemical characterization of Co doped CrO_x, in order to make it more stable and improve the high-rate behavior of chromium oxides.

2. Experimental

Crystalline Co_yCrO_x ($y = 0.1$, 0.2, 0.3, 0.4, 0.5) were prepared by heating a mixture of CrO_3 (Aldrich, 99.9%), $Co(C_2O_4) \cdot 2H_2O$ (Aldrich, 99.9%) and a small amount of chemical additive (2.0% $(NH_4)_2SO_4$ (Aldrich, 99.99%)) in an autoclave under high pressure of oxygen for 24 h [8]. The additive was added to increase the dispersive state of chromium oxides. This was followed by leaching five times with deionized water and drying in a vacuum oven at 120°C for 20 h. The chemical lithiation of $Co_{0.2}CrO_x$ was carried out by the reaction shown in Eq. (1).

$$3LiI + 2Co_{0.2}CrO_x \rightarrow 2LiCo_{0.2}CrO_x + LiI_3 \quad (1)$$

Lithium in lithiated chromium oxide was quantitatively determined by flame photometry. The method chosen for chromium determination is that of Meier et al. [16]. The procedure used has been previously described [17].

When CrO_x prepared under high oxygen pressure is cycled between 4.0 and 2.0 V vs. Li/Li Cr(VI) reduces only to Cr(V) with very high reversibility and stable capacity [11]. Thus, it is possible to reduce Cr(VI) to Cr(V) with structure retention while structural breakdown is expected by reduction to Cr(III). From the capacity of the initial charge curve and the amount of chromium, cobalt and lithium in the active material, the sum of the oxidation states of Co and Cr in $LiCo_{0.2}CrO_x$ was estimated to be +5.

$Co_{0.2}CrO_x$ was lithiated by stirring it in the solution of LiI (Aldrich) dissolved in 100 ml acetonitrile (Aldrich) solvent with ultra pure helium as purging gas. The lithiated product was leached with anhydrous acetonitrile and dried at 80°C for 10 h in a vacuum oven.

A roller-pressed round thin film cathode was prepared from active material ($Co_{0.2}CrO_x$ or $LiCo_{0.2}CrO_x$), carbon black and binder (PTFE) in a weight ratio 1:0.1:0.05. Electrochemical characterization of the cathode materials was performed in Swagelok® three electrode cells (T-cell). The anode and reference electrodes were discs of lithium foil, separator was a sheet of Whatman™ glass fiber filter paper and electrolyte was 1 M $LiPF_6$ in a 1:1:3 mixture of propylene carbonate (PC), ethylene carbonate (EC), and dimethyl carbonate (DMC). Other details regarding the fabrication of electrodes and cells are discussed in detail elsewhere [4,5,11].

Electrochemical impedance spectroscopy (EIS) experiments were carried out at open circuit potential on $Co_{0.2}CrO_x$ and $LiCo_{0.2}CrO_x$ after cycling the electrodes certain number of times. The X-ray diffraction (XRD) patterns were collected with a Rigaku 405S5 X-ray diffractometer using CuKα radiation. Cyclic Voltammograms were obtained at a scan rate of 0.1 mV/s over a potential range of 2.0–4.2 V vs. Li/Li^+. The cell performance was evaluated galvanostatically at current density of 0.5 mA/cm^2 at room temperature. The cells were cycled (charge–discharge) on Bitrode (Bitrode®, MO, USA) cycler within the cut-off potentials.

3. Results and discussion

3.1. Structure of the oxides

The synthesized Co_yCrO_x are black powders with particle size 1.0–8.5 μm. The X-ray diffraction patterns of both lithiated and non-lithiated Co doped CrO_x, and the comparison with those of undoped CrO_x are shown in Fig. 1a and b. The diffractograms are in good agreement with the literature data. The d-spacing for CrO_x is very close to that

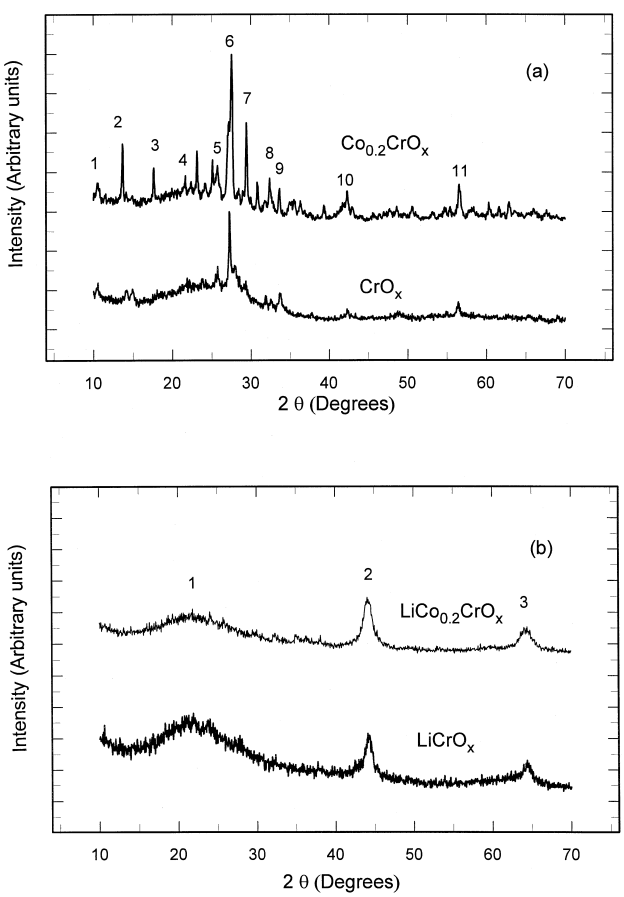

Fig. 1. X-ray diffraction patterns for (a) CrO_x and $Co_{0.2}CrO_x$, and (b) $LiCrO_x$ and $LiCo_{0.2}CrO_x$. The numbers above the peaks refer to peak numbers in Tables 1 and 2. The crystallinity of the oxide host lattice suffers severely on lithiation.

Table 1
Comparison of X-ray diffraction data for CrO_x and $Co_{0.2}CrO_x$

Peak no.	CrO_x		$Co_{0.2}CrO_x$	
	d-spacing (Å)	Relative intensity	d-spacing (Å)	Relative intensity
1	8.373	0.256	8.373	0.252
2	6.601	0.174	6.457	0.477
3	5.061	0.192	5.019	0.338
4	4.091	0.249	4.097	0.291
5	3.456	0.346	3.456	0.351
6	3.268	0.647	3.232	1.000
7	3.039	0.265	3.029	0.598
8	2.752	0.165	2.751	0.276
9	2.660	0.198	2.660	0.216
10	2.136	0.110	2.135	0.201
11	1.627	0.138	1.626	0.240

of the γ-oxide identified by Wilhelmi [18]. Some additional peaks are present in the diffractogram of $Co_{0.2}CrO_x$. None of these peaks were identified as a known species by the available powder X-ray diffraction data [19].

Table 1 lists the values of d-spacing (Å) and relative intensity from X-ray diffractometry for both CrO_x and $Co_{0.2}CrO_x$. The relative intensity is defined as

$$\text{Relative Intensity} = \frac{\text{Intensity of } CrO_x \text{ or } Co_{0.2}CrO_x \text{ peak}}{\text{Maximum intensity of } Co_{0.2}CrO_x \text{ peak}} \quad (2)$$

The maximum intensive peak for $Co_{0.2}CrO_x$ is peak No. 6 as shown in Fig. 1a. It is clear from the results presented in Table 1 that the doping of cobalt makes the material more crystalline and reduces the d-spacing. For example, the intensity of the highest peak (No. 6) for CrO_x is only 64.7% of that for $Co_{0.2}CrO_x$, and the d-spacing of this peak for $Co_{0.2}CrO_x$ is 3.232 Å which is smaller than the d-spacing of 3.268 Å for the strongest peak of CrO_x. More work is being done to understand the structural differences between pure and Co doped CrO_x which will be subject of future publication.

Comparison of the diffractograms (Fig. 1b) indicates that the crystallinity of the oxide host lattice suffers severely on chemical lithiation. The oxides undergo the transformation toward less crystalline and the d-spacing totally changes during lithium insertion (Table 2). In fact, the lithiation results in a character of amorphism (peak No. 1 in Fig. 1b). Only a very weak order was observed by the appearance of peaks No. 2 and 3 in Fig. 1b.

Table 2
Comparison of X-ray diffraction data for $LiCrO_x$ and $LiCo_{0.2}CrO_x$

Peak no.	$LiCrO_x$		$LiCo_{0.2}CrO_x$	
	d-spacing (Å)	Intensity	d-spacing (Å)	Intensity
1	4.04	vw	4.04	vw
2	2.05	m	2.05	m
3	1.45	w	1.45	w

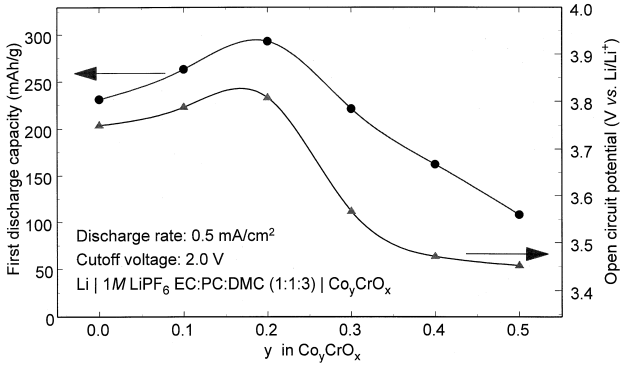

Fig. 2. The first discharge capacity (ordinate left) and open-circuit potential (ordinate right) as a function of cobalt content in the chromium oxides. $Co_{0.2}CrO_x$ exhibit highest capacity and open-circuit potential.

Cobalt doped CrO_x were synthesized with different amount of Co ($y = 0.1$, 0.2, 0.3, 0.4, and 0.5) to optimize the Co content in Co_yCrO_x. All the synthesized cobalt doped chromium oxides samples were characterized by galvanostatic charge–discharge experiments over voltage range of 2.0–4.2 V. $Co_{0.2}CrO_x$ exhibited highest capacity (more than 250 mA h/g) when cycled at the rate 0.5 mA/cm^2. Other samples show relatively low capacity, say, less than 200 mA h/g. Fig. 2 shows first discharge capacity and open circuit potential of synthesized oxides as a function of cobalt content in the oxides. It is seen that the higher the open circuit potential of the nonlithiated oxides, the higher the initial discharge capacity. Because $Co_{0.2}CrO_x$ showed the best cycling performance, it was decided to focus only on $Co_{0.2}CrO_x$ and lithiated $Co_{0.2}CrO_x$. The performance of $Co_{0.2}CrO_x$ samples will also be compared with undoped CrO_x.

3.2. Cycling performance

It is very important to determine whether the structure of the Co doped chromium oxides is stable in the entire intercalation range or not. The cyclic voltammograms (Fig. 3) were carried out between 2.0 and 4.2 V vs. Li/Li$^+$ at a

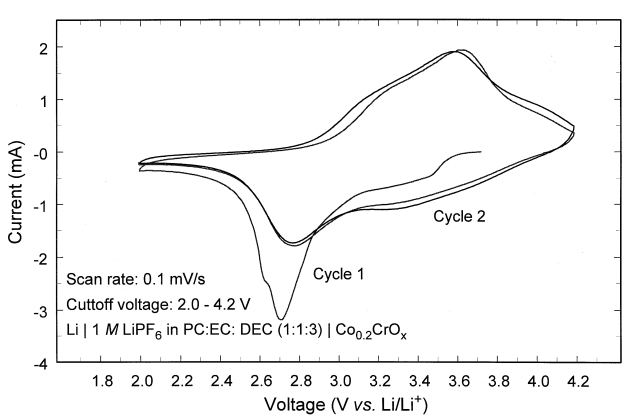

Fig. 3. Cyclic voltammograms (first and second cycle) of Li/$Co_{0.2}CrO_x$ cell at scan rate of 0.1 mV/s. $Co_{0.2}CrO_x$ is reversible in the entire intercalation range.

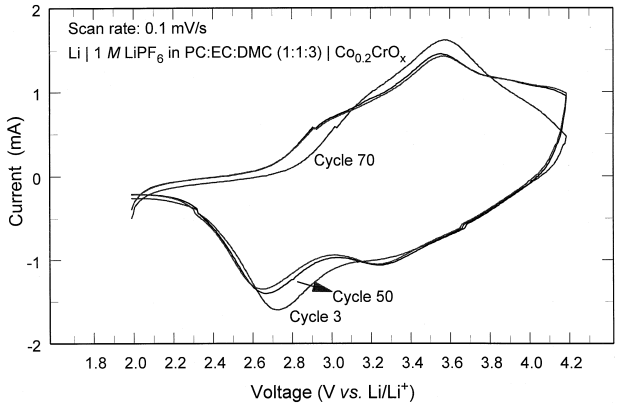

Fig. 4. Cyclic voltammograms for $Li/Co_{0.2}CrO_x$ cells after 3, 50, and 70 cycles. Scan rate: 0.1 mV/s.

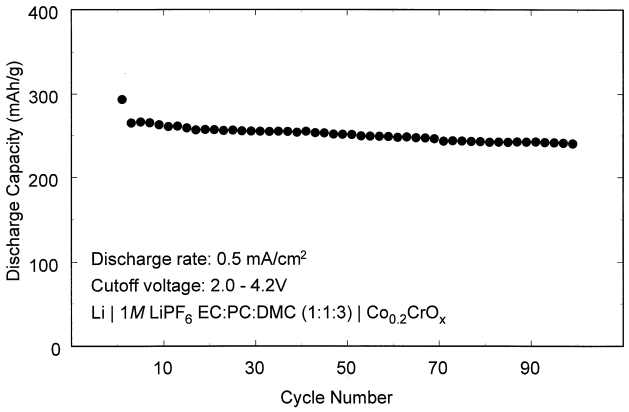

Fig. 6. Variation in the discharge capacity as a function of cycle number for $Li/Co_{0.2}CrO_x$ cells. The cells were cycled at 0.5 mA/cm^2 between 2.0 and 4.2 V.

scan rate of 0.1 mV/s to confirm the reversibility of $Co_{0.2}CrO_x$. A large peak was observed at 2.7 V during first intercalation reaction. During subsequent intercalation and de-intercalation reactions, peaks are observed at 2.7 and 3.5 V, respectively. The second and subsequent peaks are smaller compared to first peak. It is clear from Fig. 3 that $Co_{0.2}CrO_x$ is reversible in the entire intercalation range (2.0–4.2 V vs. Li/Li^+). The capacity loss during cycling was very small after first cycle.

To examine the stability of electrochemical reversibility of $Co_{0.2}CrO_x$ during cycling, cyclic voltammograms were measured after different number of cycles of galvanostatic charge–discharge. Fig. 4 shows the cyclic voltammograms after 3, 50, and 70 cycles. It is clear from the figure that the shape of cyclic voltammogram change only slightly after 70 cycles. The cathodic current peak at 3.25 V becomes more apparent after cycling, indicating that the intercalation reaction at 3.25 V is intensified to a certain extent after extended cycling. At the same time, the cathodic current peak at 2.7 V somewhat lessens. However, the electrode was still reversible in the entire intercalation range.

The galvanostatic charge–discharge curves for $Co_{0.2}CrO_x$ composite electrodes are shown in Fig. 5. The cells were charged and discharged at the rate of 0.5 mA/cm^2 between 2.0 and 4.2 V vs. Li/Li^+. Only one plateau was observed during both charge and discharge. As expected, big capacity loss was observed between first and second discharge. During the subsequent cycles, the capacity loss observed was much less. The initial discharge capacity of $Co_{0.2}CrO_x$ is 290 mA h/g, which decreases to 250 mA h/g at the end of 20 cycles. The reduction of $Co_{0.2}CrO_x$ gives rise to a voltage plateau at approximately 3.0 V vs. Li/Li^+. Fig. 6 shows the change in discharge capacity of $Co_{0.2}CrO_x$ as a function of number of cycles. The capacity after 100 cycles is 240 mA h/g. It is clear from the figure that doping with Co in the structure of CrO_x helps in stabilizing the structure and reduces the capacity fade observed during cycling. The excellent capacity retention observed in Fig. 6 is particularly noticeable if we take into account that we are working with a Li metal anode and that the well known loss of battery performance results from the poor reconstruction of the lithium surface with cycling.

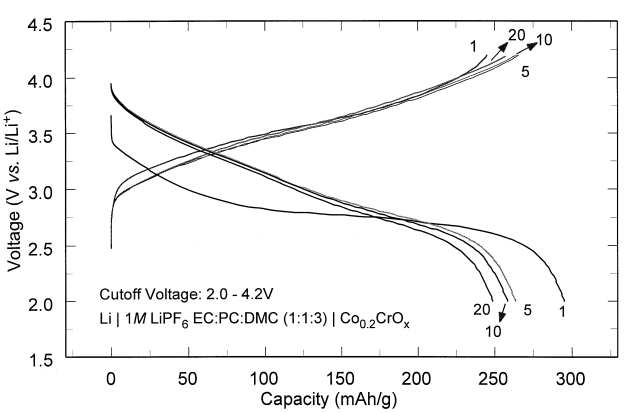

Fig. 5. Galvanostatic charge–discharge profiles for $Li/Co_{0.2}CrO_x$ cells. The numbers on the figure refer to cycle number.

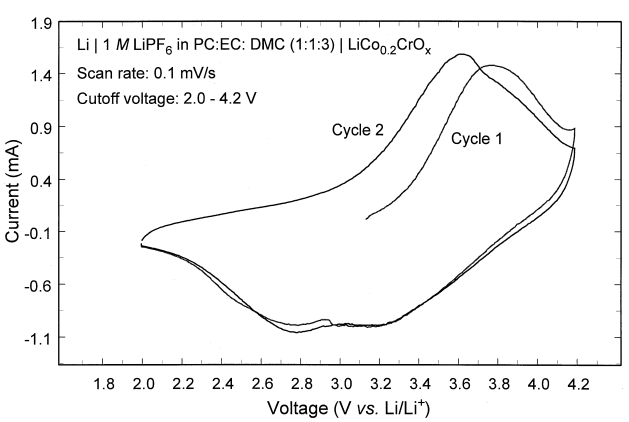

Fig. 7. Cyclic voltammograms (first and second cycle) of $Li/LiCo_{0.2}CrO_x$ cells at scan rate 0.1 mV/s. $LiCo_{0.2}CrO_x$ is reversible in the entire intercalation range.

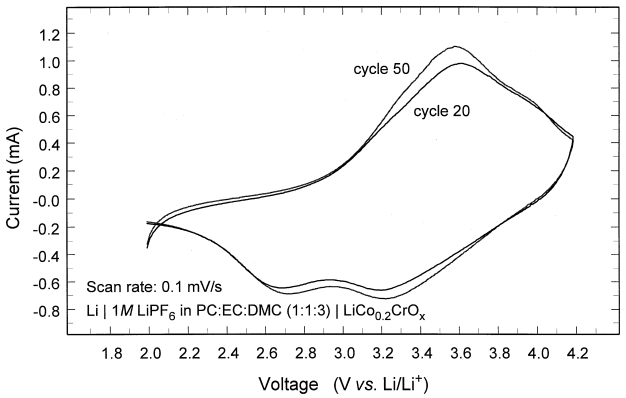

Fig. 8. Cyclic voltammograms for $LiCo_{0.2}CrO_x$ after 20 and 50 cycles. Scan rate: 0.1 mV/s.

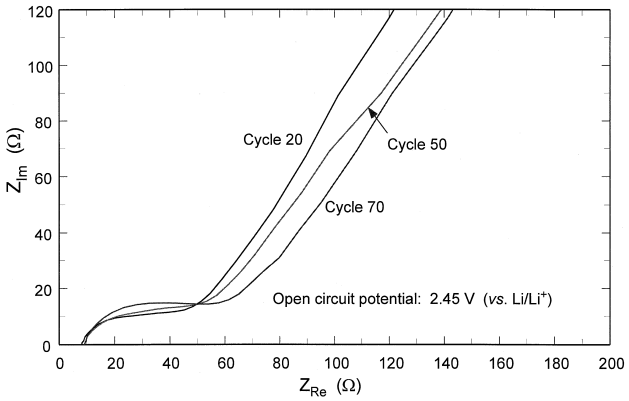

Fig. 10. Nyquist plots for $Co_{0.2}CrO_x$ cathode after 20, 50, and 70 cycles at open-circuit potential.

In order to check the reversible behavior of $LiCo_{0.2}CrO_x$, cyclic voltammograms were carried out between 2.0 and 4.2 V at 0.1 mV/s as shown in Fig. 7. First de-intercalation peak was observed at 3.7 V while the subsequent peaks were observed at 3.5 V vs. Li/Li^+. The intercalation peaks were observed at 2.8 V. It is seen from the cathodic process that a very small capacity loss was observed between first and second cycle. The cyclic voltammograms of $LiCo_{0.2}CrO_x$ does not undergo much change after extended cycling. As shown in Fig. 8, although the capacity at cycle 50 drops a little compared with cycle 20, the shape of the curves remains almost the same, indicating that the structure is reversible even after extended cycling. Fig. 9 shows the first five galvanostatic charge–discharge curves of $LiCo_{0.2}CrO_x$ when cycled between 2.0 and 4.2 V vs. Li/Li^+ at 0.5 mA/cm^2. It is seen from the figure that the discharge capacity decreases from 230 mA h/g to 215 mA h/g during the first five cycles.

3.3. Electrochemical impedance spectroscopy

EIS experiments were carried out at open circuit potential on $Co_{0.2}CrO_x$ and $LiCo_{0.2}CrO_x$ in Swagelok three-electrode cells (T-cells). The anode and reference electrodes were discs of lithium foil. The impedance covered the frequency range from 0.005 Hz to 20 kHz with an AC voltage amplitude of 5 mV. Fig. 10 shows the Nyquist plots for $Co_{0.2}CrO_x$ at open circuit potential 2.45 V vs. Li/Li^+ after 20, 50, and 70 cycles. The ohmic resistance was estimated as the value of intersection of the high frequency end of the depressed semicircle with the abscissa. The interfacial impedance was estimated as the difference of intersections of the fitted semicircle with the abscissa. A small increase in ohmic resistance was observed between 20 cycles (8.21 Ω) and 70 cycles (9.12 Ω). The interfacial impedance increases from 33.2 Ω (20 cycles) to 43.5 Ω after 70 cycles. This increase of impedance during cycling is in accordance with the slight capacity fade observed for cobalt doped chromium oxide as shown in Fig. 6.

The Nyquist plots are shown in Fig. 11 for $LiCo_{0.2}CrO_x$ at open circuit potential 2.71 V vs. Li/Li^+ after 10, 40, and 50 cycles. Similar to $Co_{0.2}CrO_x$, a small increase in ohmic resistance was observed between 20 cycle (7.26 Ω) and 50 cycles (8.91 Ω). The interfacial impedance increases from 22.7 Ω (cycle 10) to 32.1 Ω after cycle 50.

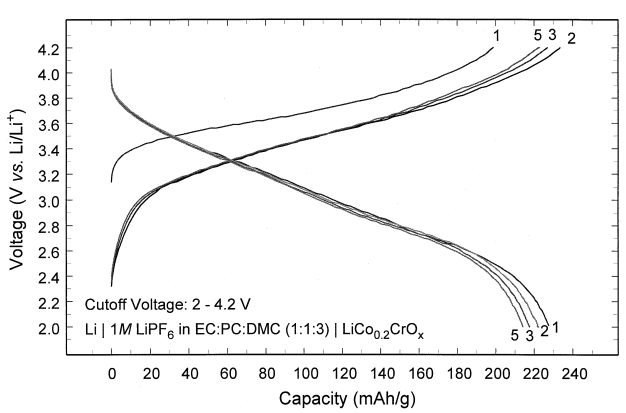

Fig. 9. Galvanostatic charge–discharge profiles for $Li/LiCo_{0.2}CrO_x$ cells. The numbers on the figure refer to cycle number.

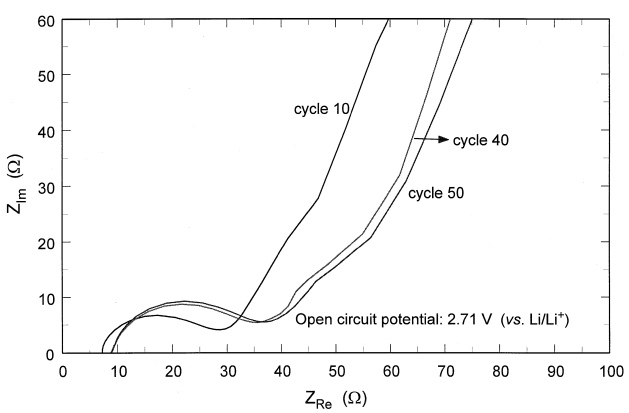

Fig. 11. Nyquist plots for $LiCo_{0.2}CrO_x$ cathode after 10, 40 and 50 cycles at open-circuit potential.

This impedance change contributes importantly to the capacity fade of the lithiated cobalt chromium oxide.

To account for the increase of internal impedance with the cycle number of the lithium/chromium oxide cells, solid electrolyte interphase (SEI) model can be employed. That is, charge–discharge cycling of the electrode results in formation of an ionically conducting but electronically insulating surface layer at electrode/electrolyte interface [20]. Across the SEI, the ion transport may be represented by the insertion ion resistance and polarization over the SEI by a capacitance in parallel. The existence of the SEI modifies the double layer capacitance, which is associated with the mobile species in the SEI. Since the double layer is confined to a small portion of the SEI, the relation that double layer capacitance is larger than SEI capacitance can be anticipated. In this case, Nyquist plot with two arcs should be observed. However, when both capacitances are very close, the Nyquist plot can no longer be separated as two distinguished arcs. The curves turn out to be one depressed semicircle as shown in Figs. 10 and 11.

3.4. Rate behavior

It is very important to characterize these materials for their rate behavior as most of the applications demand high-rate discharges during normal operation. The cycling rates were varied over the course of the experiment to examine the effect of high discharge rates on capacity and cycle life. The high-rate behavior of CrO_x and $LiCrO_x$ was found to be poor, which was attributed to small diffusion coefficient of Li in CrO_x solid [10–12]. Addition of small amount of Co in the CrO_x structure helps in improving the high rate behavior of these oxides. Fig. 12 shows the charge–discharge profiles of $Co_{0.2}CrO_x$ when discharged at 2.0 mA/cm^2 (ca. 1.5 C). The discharge capacity is as high as 170 mA h/g, and the capacity fade is very small during cycling. The rate capability of these electrode materials was also determined by obtaining a signature curve.

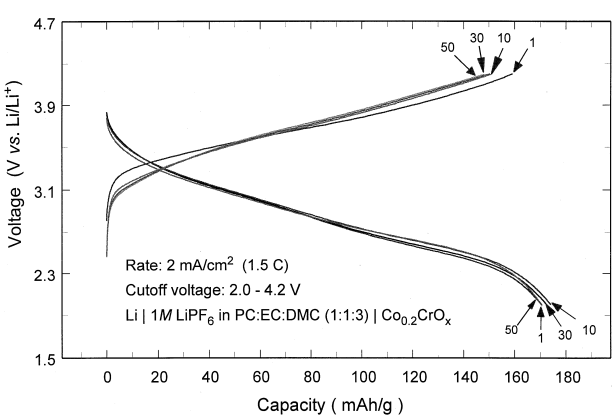

Fig. 12. High rate charge–discharge profiles for $Li/Co_{0.2}CrO_x$ cells between 2.0–4.2 V. The numbers on the figure refer to cycle number.

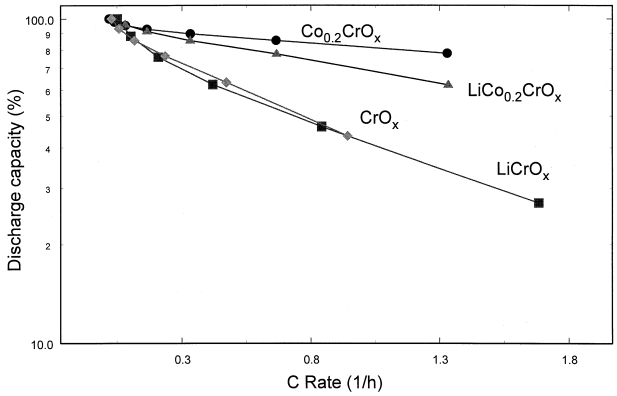

Fig. 13. The discharge capacity as a function of various discharging rates for lithiated and non-lithiated cobalt doped chromium oxides. The high rate behavior of pure chromium oxides is also shown for comparison.

In this method the cell is discharged at highest rate from the fully charged state. The cell is then allowed to rest for a specified time and then discharge at rate smaller than the first rate. The above process is repeated until the lowest discharge rate has been used. Fig. 13 summarizes the high rate behavior of lithiated and non-lithiated pure and Co doped CrO_x. As shown in Fig. 13 more than 85% capacity is observed for $Co_{0.2}CrO_x$ and more then 75% capacity is observed for $LiCo_{0.2}CrO_x$ at 0.65 C rate. The high-rate behavior of CrO_x and $LiCrO_x$ is also shown in the figure, which is poor compared to Co doped CrO_x.

4. Conclusions

The lithiated and non-lithiated cobalt doped chromium oxides were found to be promising cathode material for secondary lithium batteries. $Co_{0.2}CrO_x$ and $LiCo_{0.2}CrO_x$ had an initial capacity of 290 and 230 mAh/g, respectively with an average discharge voltage of 3.0 V. Both lithiated and non-lithiated Co doped CrO_x were found to be reversible in the entire intercalation range (2.0–4.2 V vs. Li/Li^+). Substituting a small amount of Co in CrO_x and $LiCrO_x$ dramatically improves the stability and rate behavior of these oxides. Co doped CrO_x exhibited more than 75% capacity at 0.65C rate. Lithiated and non-lithiated Co doped CrO_x can be used as positive electrodes in secondary lithium batteries with carbon and lithiated carbon as negative electrodes, respectively.

Acknowledgements

The authors gratefully acknowledge the financial support provided by DOE Division of Chemical Sciences, Office of Basic Energy Sciences G.M. DE-FG02-96ER 146598.

References

[1] K. Mizushima, P.C. Jones, P.J. Wiseman, J.B. Goodenough, Solid State Ionics 3/4 (1981) 171.
[2] J.R. Dahn, U. Von Sacken, M.R. Jukow, H. Al-Janaby, J. Electrochem. Soc. 138 (1991) 2207.
[3] J.M. Tarascon, D. Guyomard, J. Electrochem. Soc. 138 (1991) 2864.
[4] P. Arora, B.N. Popov, R.E. White, J. Electrochem. Soc. 145 (1998) 807.
[5] D. Zhang, B.N. Popov, R.E. White, J. Power Sources 76 (1998) 81.
[6] C. Sigala, D. Guyomard, A. Verbaere, Y. Piffard, M. Tournoux, Solid State Ionics 81 (1995) 167.
[7] M.E. Spahr, P. Novak, W. Scheifile, O. Haas, R. Nesper, J. Electrochem. Soc. 145 (1998) 421.
[8] F. Coustier, S. Passerini, W.H. Smyrl, J. Electrochem. Soc. 145 (1998) L73.
[9] J. Dai, S.F.Y. Li, Z. Gao, K.S. Siow, J. Electrochem. Soc. 145 (1998) 3057.
[10] P. Arora, G. Zheng, B.N. Popov, R.E. White, Abstract No. 90, The Electrochemical Society Meeting Extended Abstracts, Vol. 97-1, Montreal, Canada, May 3–8, (1997).
[11] P. Arora, D. Zhang, B.N. Popov, R.E. White, Electrochem. Solid-State Lett. 1 (1998) 249.
[12] B.N. Popov, D. Zhang, R.E. White, Abstract No. 52, The Electrochemical Society Meeting Extended Abstracts, Vol. 98-1, San Diego, CA, May 3–8, 1998.
[13] J.O. Bessenhard, R. Schollhorn, J. Electrochem. Soc. 124 (1977) 968.
[14] R. Koksbang, S. Yde-Andersen, K. West, S. Skaarup, Solid State Ionics 28–30 (1988) 868.
[15] J.O. Bessenhard, M. Schwake, J. Power Sources 26 (1989) 309.
[16] D.J. Meier, R.T. Myers, E.H. Swift, J. Am. Chem. Soc. 71 (1949) 2340.
[17] H.A. Laitinen, J.H. Propp, Anal. Chem. 41 (1969) 645.
[18] K.-A. Wilhelmi, Acta Chemica Scandinavica 22 (1968) 2565.
[19] Powder Diffraction File, Apphabetical Index, Inorganic Phases, JCPDS International Center for Diffraction Data 1985, USA, (1985).
[20] E. Peled, J. Electrochem. Soc. 126 (1979) 2047.